(Received 15 September 2025, Accepted 31 October 2025, Scheduled 15 November 2025)

A Dual-Band Frequency-Dependent Beam Scanning Antenna System for RFID and WLAN Applications

Anweya Das, Atrisha Biswas, Ahana Gupta, Soham Bhattacharya, and Sayan Sarkar*

Department of Electronics and Communication Engineering, Institute of Engineering & Management, Salt Lake, Kolkata, India

ABSTRACT: This paper presents a single-layered dual-band microstrip patch antenna with periodic sinusoidal slots. The antenna operates within 860–930 MHz and 2400–2500 MHz. The first band encompasses both the European and North American UHF-RFID bands while the second band covers the 2.45 GHz Microwave-RFID/WLAN band. Moreover, the presence of the sinusoidal slots helps the antenna exhibit frequency-dependent beam scanning within the 2.45 GHz band. Four such antenna units are placed close to each other with different orientations to create a 2×2 antenna system. This system can detect UHF-RFID tags using both horizontal and vertical polarizations. It can also perform frequency-dependent beam scanning with horizontal polarization in the yz-plane and vertical polarization in the xz-plane. The beam maximum scans from -30° to 31° in the yz-plane and -32° to 29° in the xz-plane.

1. INTRODUCTION

The use of Radio Frequency Identification (RFID) technology has become widespread in various different sectors throughout the world [1]. In the Ultra high frequency (UHF) region, we have the European band spanning 865–868 MHz and the North American band spanning 902–928 MHz. The Microwave-RFID band coincides with the 2.45 GHz band and is usually used for short distance and high-speed tag detection. A plethora of RFID readers can be found in literature [2–20]. Out of them, many dual-band RFID readers can be identified [2–5, 7–11, 14–20]. These mostly operate within the UHF-RFID band and 2.45 GHz WLAN band.

Although each of the above RFID readers has unique features which make them useful, there are still a few areas of improvement. Firstly, most of the UHF-RFID readers cover either the European or North American UHF-RFID bands, but not both simultaneously. The antenna designed in [2] can cover both, but requires manual intervention in the form of changing the superstrates to change the operating band. Secondly, dual-band RFID readers with beam scanning ability are not found in literature. The use of beam scanning can enhance the usefulness of an RFID reader by a great extent.

In this paper, a 2×2 multiport microstrip patch antenna arrangement is presented. The building block of this arrangement is a square microstrip patch with periodic sinusoidal slots. This patch has two operational bands. The first band spans 860–930 MHz (7.8%), and the second spans 2400–2500 MHz (4.08%). Therefore, the patch can cover both the European and North American UHF-RFID bands simultaneously. Within the 2.45 GHz band, the antenna can alternately be used to scan Microwave-RFID tags or send tag information to base stations. The main highlight of the proposed structure is its frequency-dependent beam scanning property within the 2.45 GHz band. This makes the antenna unique as an RFID reader. By arranging four such modified square patches in different orientations, a single-layered, dual-linearly polarized antenna system is designed. The 2×2 system can scan both the *xz*- and *yz*-planes within the 2.45 GHz band. Moreover, the antenna gains hover around 7 dBi and 10.5 dBi within the first and second bands respectively with total efficiencies falling within the 75–85% region in both bands. The dimensions of the system are on the larger side, making it more suitable for desktop reader applications which do not have stringent size constraints.

* Corresponding author: Sayan Sarkar (sayansarkar0794@gmail.com).

2. MICROSTRIP PATCH WITH PERIODIC SINUSOIDAL SLOTS

Simulations are performed using Computer Simulation Technology (CST) Microwave Studio. The patch is designed using Copper, and the substrate is designed using a 1.52 mm thick FR-4 ($\varepsilon_r = 4.2$; $\tan\delta = 0.025$).

2.1. Patch Geometry

The base antenna chosen for this paper is a square patch antenna with coaxial feed lying in the *xy*-plane. If the antenna centre coincides with the origin of a cartesian coordinate system, the feed location can be given by the point $(15, -15)$. The length of the patch ($L1$) is chosen such that it corresponds to $\approx 0.48\lambda_g$ ($0.24\lambda_0$) at 865 MHz and $\approx 1.37\lambda_g$ or $0.685\lambda_0$ at 2450 MHz. Here, the free-space and guided wavelengths are denoted using λ_0 and λ_g, respectively. 2450 MHz is close to the third harmonic of the square patch.

The base antenna is then modified by adding twelve horizontal sinusoidal slots with a fixed spacing. The modified patch antenna is shown in Fig. 1. The analytical curve used to design the slots is $y = \sin(x)$; $-L1/2 < x < L1/2$. The first sinusoidal slot ($i = 0$) is designed along the x-axis ($y = 0$) with

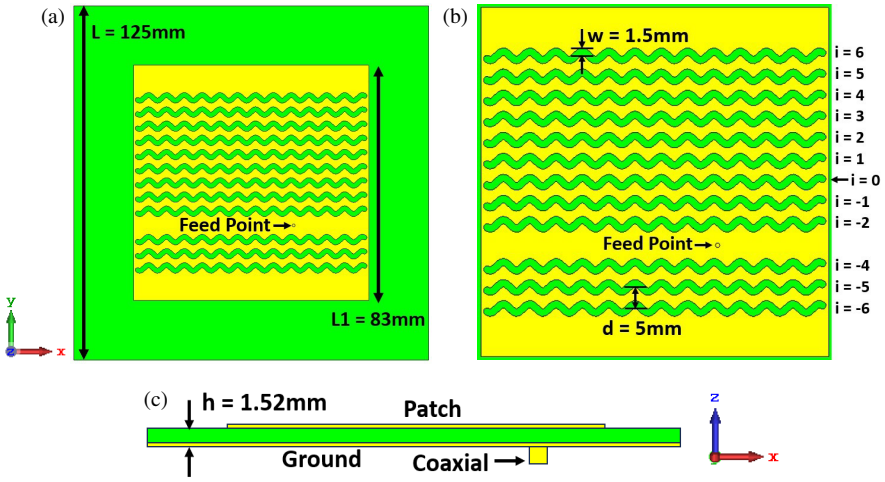

FIGURE 1. (a) Square patch with periodic sinusoidal slots. (b) Expanded view of the patch with slot dimensions. (c) Side view.

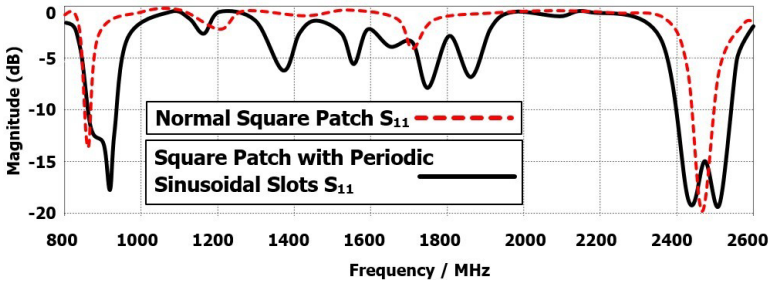

FIGURE 2. Simulated S_{11} versus frequency for the normal square patch and modified square patch.

a width (w) of 1.5 mm. The six slots above $i = 0$ are translated versions of $i = 0$ with a spacing (d) of 5 mm. Similarly, the five slots below $i = 0$ are also translated versions with the same spacing. The slot at position $i = -3$ is omitted because of the feed location ($15, -15$) along that given line. The square patch can accommodate two more slots ($i = 7$ and $i = -7$). However, the addition of these slots does not influence the antenna characteristics, and they are therefore not included. The feed location was not changed throughout the design since the antenna continued exhibiting good matching.

2.2. Modified Antenna Characteristics

The S_{11} of this modified design is shown in Fig. 2 (black solid curve) and compared with the S_{11} of the normal square patch. There is a significant broadening of the $S_{11} \leq -10$ dB regions compared to the normal patch. The slotted patch antenna has -10 dB S_{11} bandwidths of 70 MHz (860–930 MHz) and 100 MHz (2400–2500 MHz). Therefore, it covers the UHF-RFID band as well as Microwave-RFID/WLAN band.

The radiation patterns of the modified antenna are shown in Fig. 3. The radiation patterns within both the bands are predominantly horizontally polarized (x-directed E-fields; *H-pol*). This is because the horizontal slots prevent the existence of y-directed surface currents. The radiation patterns at both 865 MHz and 915 MHz are predominantly broadside in nature. The radiation patterns within the 2400 MHz band show a frequency-dependent beam scanning tendency in the *yz*-plane. At 2400 MHz, the beam maximum is located at $\theta = 0°$. The beam maximum shifts to the left as frequency increases. The beam maximum is located at $\theta = -12°$ (negative sign is used to indicate a left tilt) for 2420 MHz, at $\theta = -24°$ for 2450 MHz and at $\theta = -31°$ for 2490 MHz. The beam maxima direction in the *yz*-plane for each of these four frequencies is shown with a blue line in Figs. 3(c)–(f).

There are two main drawbacks of this modified antenna. Firstly, the antenna operates with a single polarization (horizontal). This limits tag detection to only horizontally aligned tags (this problem does not exist for circularly polarized tags). Secondly, the beam scanning is only along the left of the *yz*-plane ($0°$ to $-31°$). These two drawbacks are overcome in the next section.

2.3. Fixing the Number of Sinusoidal Slots

To fix the total number of sinusoidal slots in the patch design, various configurations of the antenna were simulated.

Three such variations are shown in Figs. 4(a)–(c). Fig. 4(a) has 9 sinusoidal slots present above the feed location; 4(b) has 5 slots above and 3 slots below the feed location; and 4(c) has 7 slots with twice the spacing. The S_{11} of the three arrangements are plotted in Fig. 4(d) along with the S_{11} of the finalized design of Fig. 1. The absence of the slots below the feed line reduces the -10 dB S_{11} bandwidth (BW) of the higher order mode. Reducing the number of slots on top leads to poor matching within the higher order mode and a right shift of the primary resonant

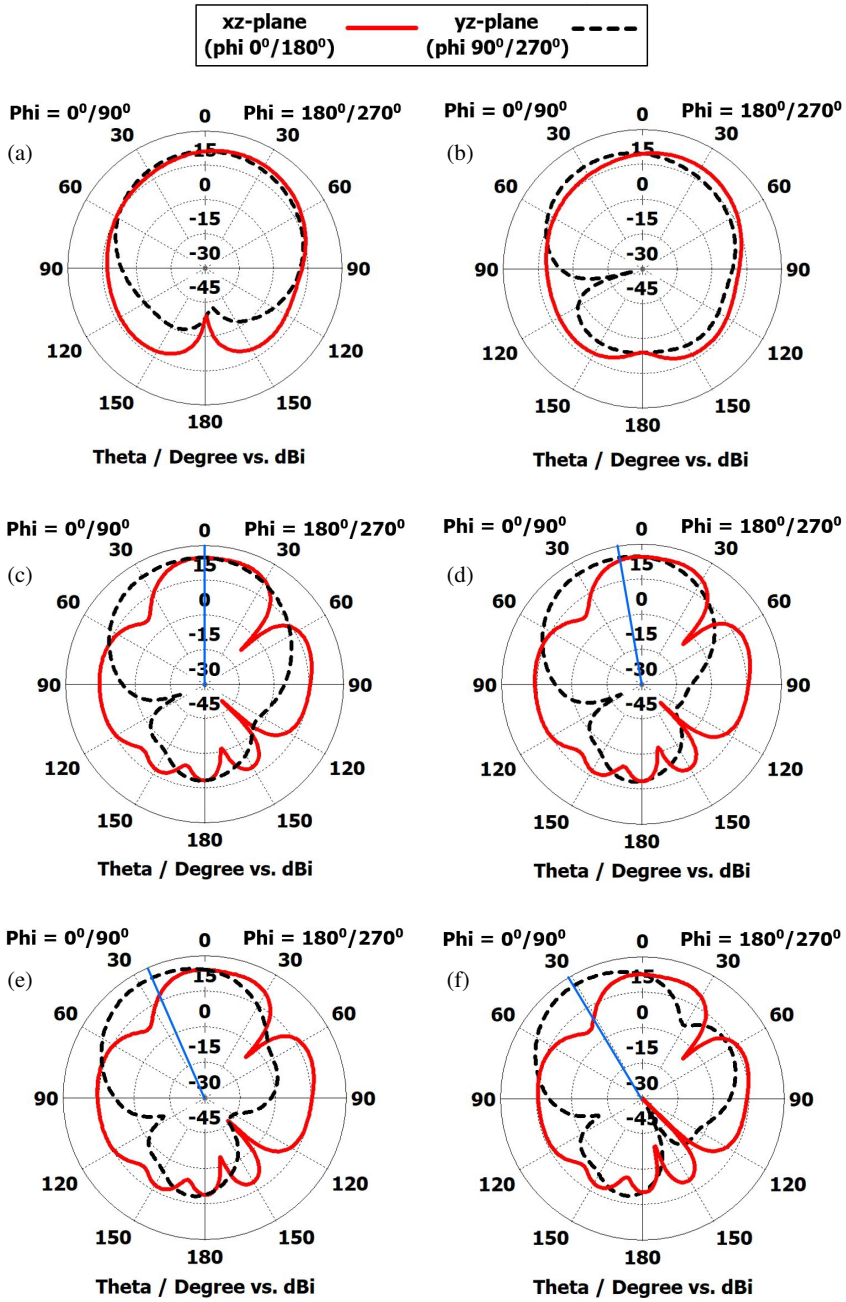

FIGURE 3. Simulated horizontally polarized radiation patterns at (a) 865 MHz, (b) 915 MHz, (c) 2400 MHz, (d) 2420 MHz, (e) 2450 MHz and (f) 2490 MHz.

band. Reducing the number of slots and doubling the slot spacing leads to reduced matching within the 2400 MHz band and a right shift of the 860 MHz band. The patch antenna with 12 sinusoidal slots is found to possess the optimum reflection coefficient for proper utilization of the UHF-RFID and WLAN bands.

3. 2 × 2 PATCH ARRANGEMENT

3.1. 2 × 2 Antenna Geometry

To remove the first drawback discussed in the previous section, a 90° rotated version of the modified patch can be used. This will result in vertical sinusoidal slots and vertical polarization (y-directed E-fields; *V-pol*). To remove the second drawback, an 180° rotated version of the patch can be used. This will result in horizontal beam scanning along the right in the yz-plane (0° to 31°). Combining these two solutions, a 2 × 2 antenna system is designed, as shown in Figs. 5(a)–(b). There are 4 modified patch antennas placed with an edge-to-edge spacing, G, of 42 mm and centre-to-centre spacing, $G1$, of 125 mm. The feed points are numbered to denote the antenna serial number. For the UHF-RFID band, Ant. 1 and 2 produce *H-pol* radiation patterns with the same shape while Ant. 3 and 4 produce *V-pol* radiation patterns with the same shape. Ant. 1/2 and Ant. 3/4

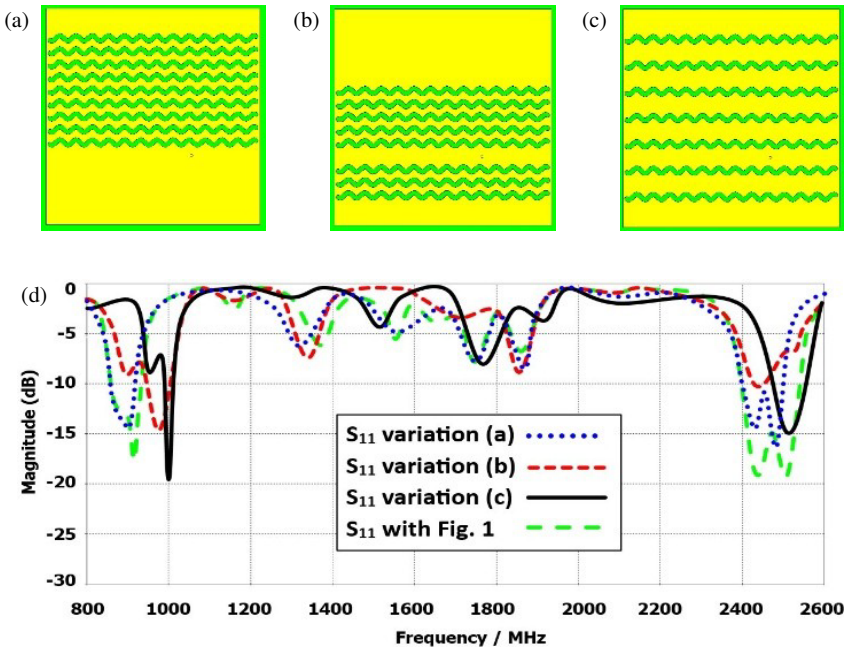

FIGURE 4. Patch with (a) no lower slots, (b) partial upper slots and (c) 7 slots with twice the spacing as original. (d) S_{11} versus frequency of the three different configurations and the original of Fig. 1.

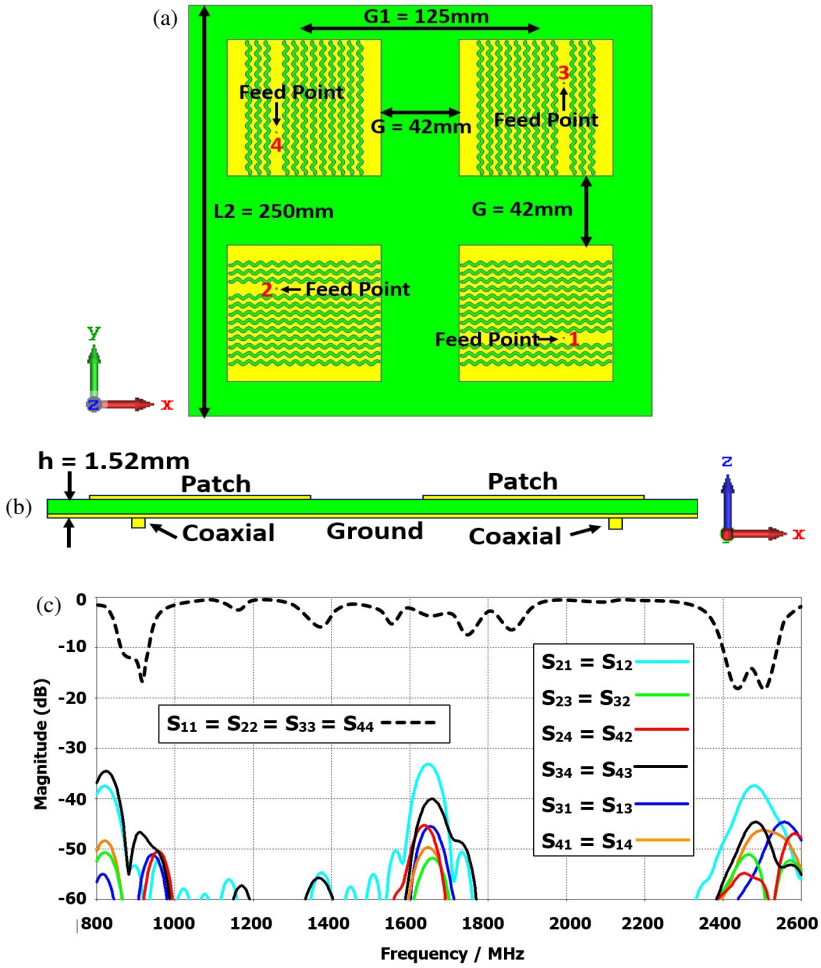

FIGURE 5. 2×2 antenna configuration (a) top and (b) side views. (c) S-parameters of the four-antenna system.

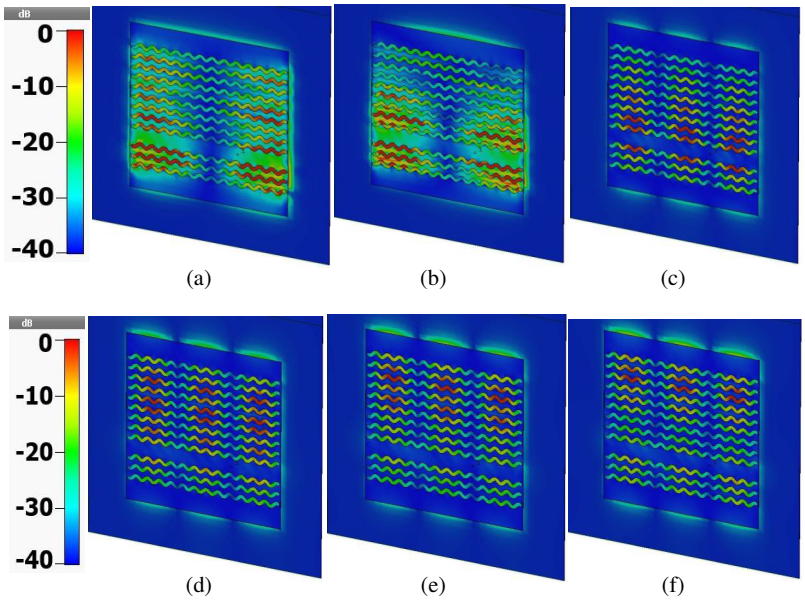

FIGURE 6. Induced surface currents on Ant. 1 at (a) 865 MHz, (b) 915 MHz, (c) 2.4 GHz, (d) 2.42 GHz, (e) 2.45 GHz and (f) 2.49 GHz.

can be used interchangeably for a complete dual-linearly polarized UHF-RFID tag scan. For the Microwave-RFID band, Ant. 1 and 2 together can scan the *yz*-plane within the range of $\pm 31^\circ$ with *H-pol*. Ant. 3 and 4 together can scan the *xz*-plane within the range of $\pm 31^\circ$ with *V-pol*. Using all four antennas, both *H*- and *V-pol* scans are achieved.

The S-parameters of the four antennas are plotted in Fig. 5(c). The reflection coefficients remain the same as the isolated antenna in Fig. 2. Moreover, the low S_{ij} values ($i \neq j$; $i, j = 1$ to 4) indicate that there is good isolation between them.

The total dimensions of the 2×2 antenna system are $0.71\lambda_0 \times 0.71\lambda_0 \times 0.004\lambda_0$ at 860 MHz and $2\lambda_0 \times 2\lambda_0 \times 0.013\lambda_0$ at 2500 MHz. The antenna size within the WLAN band is sacrificed to some extent to achieve the complete beam-scanning characteristic.

3.2. Induced Surface Currents

The surface currents induced on Ant. 1 at six different frequencies within the two operating bands are plotted in Fig. 6. The currents are spread across almost the entire patch at 865 MHz and 915 MHz (Figs. 6(a)–(b)). This gives rise to the broadside patterns within the UHF-RFID band. The location of the current maxima moves up vertically along the patch (in the y-direction) with increasing frequency. It starts in the middle at 2400 MHz and moves close to the top at 2490 MHz (Figs. 6(c)–(f)). This indicates that the beam maximum is also moving towards the top from its central (broadside) location.

3.3. Beam Scanning Plots

The radiation patterns of Ant. 2, 3, and 4 can be visualized by observing the radiation pattern of Ant. 1 plotted in Fig. 3 and the orientation of the antenna under consideration. For instance, the *xz* and *yz* patterns of Ant. 2 are mirror images of the *xz* and *yz* patterns of Ant. 1 since Ant. 2 is an 180° rotated version of Ant. 1. Similarly, the *xz* pattern of Ant. 3 is a mirror image of the *yz* pattern of Ant. 1, and the *yz* pattern of Ant. 3 is a mirror image of the *xz* pattern of Ant. 1. This is because Ant. 3 is a 90° rotated version of Ant. 1. Finally, the *xz* pattern of Ant. 4 (-90° rotated version of Ant. 1) is the same as the *yz* pattern of Ant. 1, and the *yz* pattern of Ant. 4 is the same as the *xz* pattern of Ant. 1. Since the radiation patterns of all the four antennas are similar, the complete radiation patterns of Ant. 2, 3, and 4 are not plotted for brevity. However, the radiation patterns in the beam scanning planes of all the four antennas are shown in Fig. 7. The average 3 dB line in each figure is calculated by averaging the peak gains of the four frequencies and subtracting 3 dB from the result.

As discussed earlier, Ant. 1 and 2 provide *H-pol* beam scanning in the *yz*-plane while Ant. 3 and 4 provide *V-pol* beam scanning in the *xz*-plane. The beam maxima for each antenna can scan approximately 30°, and the 3 dB beamwidth scans approximately 90°.

The beam scanning occurs due to the phase shift of the induced fields while they are flowing along the length of the antenna and interacting with the sinusoidal slots. The phase shift between adjacent sinusoidal slots can be calculated using $\Phi = 2\pi d/\lambda_g$, where d = slot spacing and $\lambda_g = \lambda_0/\sqrt{\varepsilon_r}$. At 860 MHz, the phase shift is $\approx 2.9^\circ$/slot while it is $\approx 3.3^\circ$/slot at 915 MHz. Similarly, the phase shift is $\approx 8.6^\circ$/slot at 2400 MHz and $\approx 9^\circ$/slot at 2490 MHz. Within the UHF-RFID band, the phase shift is minimal, and the radiation pattern maxima does not shift with frequency. This can also be understood considering that the slot spacing is only $0.0085\lambda_g$ at 860 MHz and $0.009\lambda_g$ at 915 MHz. Within the WLAN band, the slot spacing is $0.024\lambda_g$ and $0.025\lambda_g$ at 2400 MHz and 2490 MHz, respectively. As the frequency increases, the phase shift increases by almost 9°/slot and tilts the maxima of the radiation pattern. This leads to the beam scanning effect within the WLAN band.

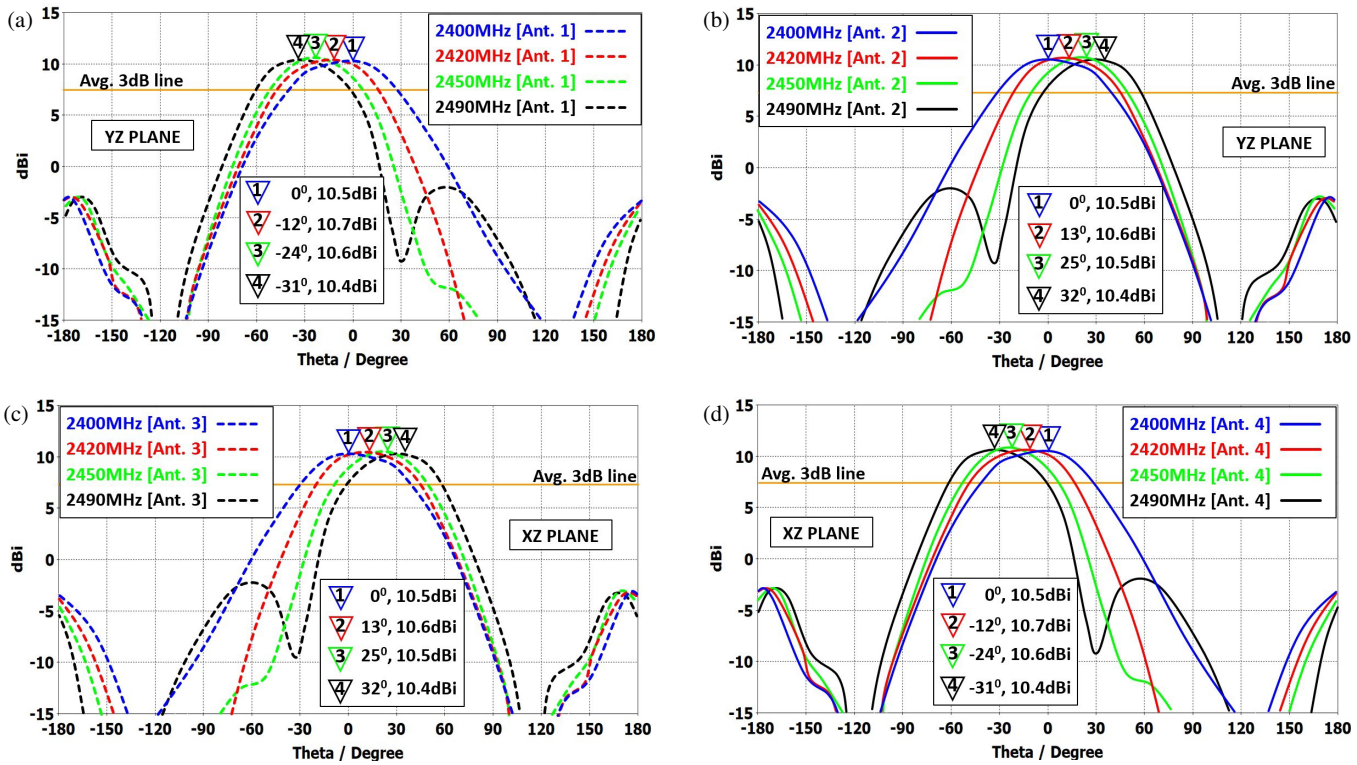

FIGURE 7. Simulated horizontally polarized beam scanning along the *yz*-plane by (a) Ant. 1 and (b) Ant. 2. Simulated vertically polarized beam scanning along the *xz*-plane by (c) Ant. 3 and (d) Ant. 4.

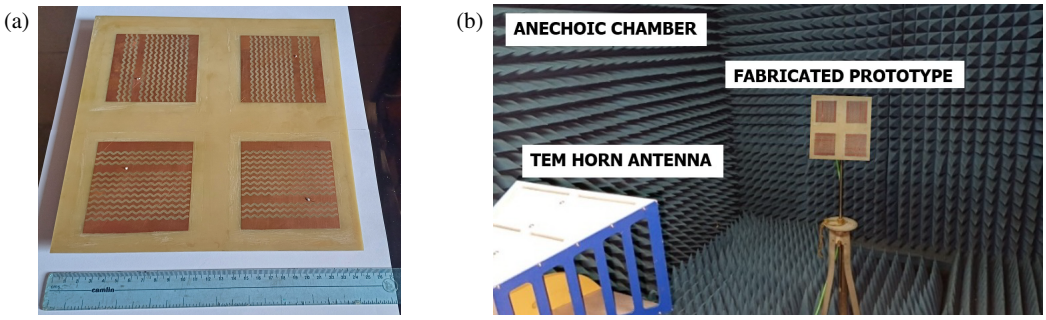

FIGURE 8. (a) Fabricated prototype and (b) measurement setup.

4. MEASUREMENTS

To validate the simulated results, a 2×2 prototype of the antenna system is fabricated. The fabricated prototype and measurement setup are shown in Fig. 8. A wideband TEM horn antenna is used for radiation pattern measurement.

The measured S-parameters are plotted in Fig. 9. The reflection coefficients of all the four antennas are nearly identical and resemble the simulated curves. The isolation between ports is also very good. The low values of the measured S_{ij} curves $(i \neq j)$ of Fig. 9(b) show that there is very little mutual coupling between the antenna elements.

The radiation patterns of the four antennas are also measured. The co- and cross-polarized patterns for Ant. 1 at the six frequencies of interest are shown in Fig. 10. The measured patterns resemble the simulated patterns of Fig. 3. It is also found that the antennas have very low cross polarization levels. The simulated and measured patterns are plotted separately to make the graphs clearer to the reader. The measured characteristics of Ant. 1 are summarized in Table 1.

The simulated and measured gains of Ant. 1 are plotted in Fig. 11. The simulated total efficiencies of Ant. 1 are also presented in the same figure. It is seen that the gain hovers close to 7 dBi within the UHF-RFID band and close to 10.5 dBi within the WLAN/Microwave-RFID band. The efficiencies lie within the 75–80% region. The gains and efficiencies of the other antennas are the same as those of Ant. 1.

The measured beam scanning characteristics of the four antennas are plotted in Fig. 12. The scanning nature is similar to the simulated results of Fig. 7. The measured scanning properties of the 2×2 antenna system are summarized in Table 2. It is seen that the beam maximum scans from $-30°$ to $31°$ $(61°)$ in the *yz*-plane (*H-pol*) and from $-32°$ to $29°$ $(61°)$ in the *xz*-

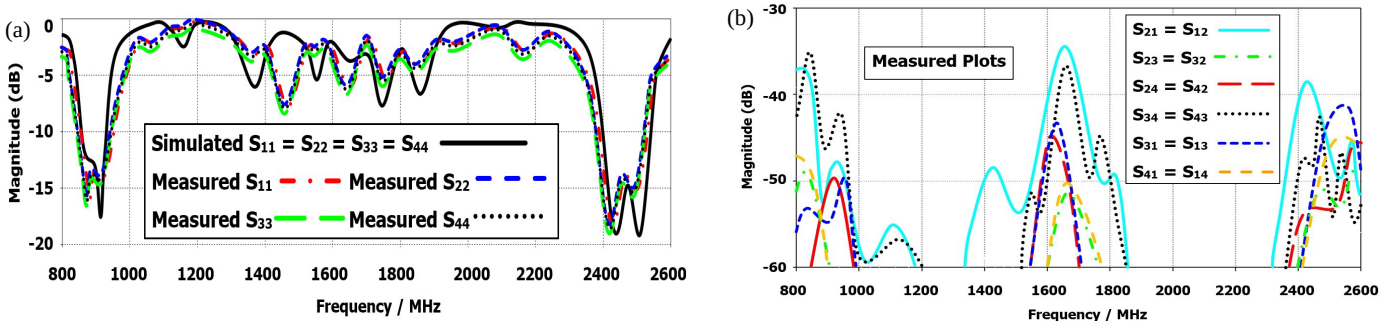

FIGURE 9. (a) Simulated versus measured reflection coefficients and (b) measured S_{ij} parameters ($i \neq j$).

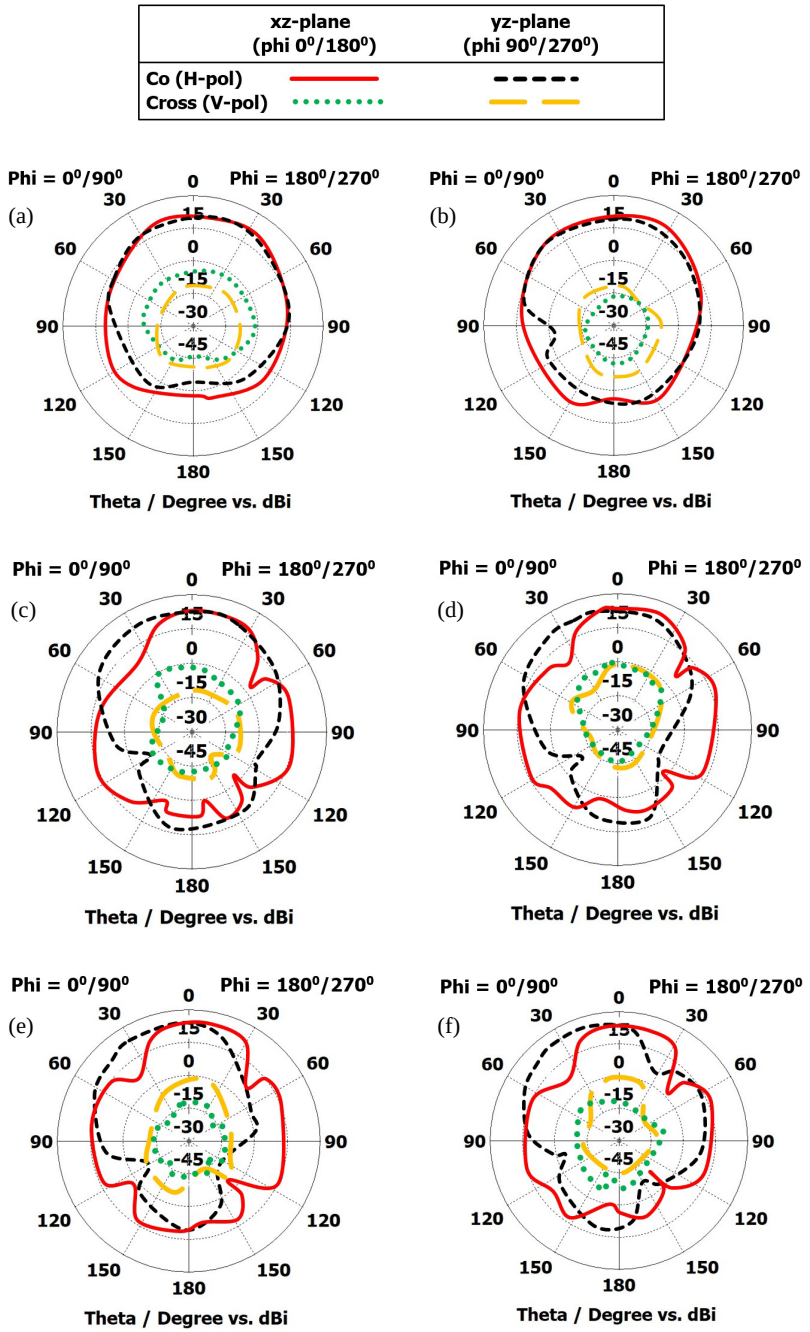

FIGURE 10. Measured co- (horizontal) and cross- (vertical) polarized radiation patterns of Ant. 1 at (a) 865 MHz, (b) 915 MHz, (c) 2400 MHz, (d) 2420 MHz, (e) 2450 MHz and (f) 2490 MHz.

TABLE 1. Radiation characteristics of Antenna 1.

Freq. (MHz)	xz-plane 3 dB beamwidth [Max. Gain]	yz-plane 3 dB beamwidth [Max. Gain]	Beam maximum direction in scanning plane (yz)
865	72° (−31° to 41°) [6.64 dBi]	87° (−40° to 47°) [6.68 dBi]	0°
914	74° (−34° to 40°) [6.74 dBi]	73° (−40° to 33°) [6.78 dBi]	0°
2400	52° (−22° to 30°) [10.43 dBi]	63° (−39° to 24°) [10.45 dBi]	0°
2420	49° (−19° to 30°) [10.82 dBi]	67° (−47° to 20°) [10.79 dBi]	−12°
2450	50° (−18° to 32°) [10.64 dBi]	62° (−52° to 10°) [10.66 dBi]	−25°
2490	48° (−21° to 27°) [10.68 dBi]	57° (−57° to 0°) [10.53 dBi]	−30°

TABLE 2. Scanning characteristics of the 2 × 2 antenna system within the 2.45 GHz band.

Scan Plane	Scan Pol.	Beam Maxima Scan Range	Beam 3 dB Scan Range
yz-plane	x-directed E-field (*H-pol*)	(−30° to 0°) Ant. 1 (0° to 31°) Ant. 2 **Total = 61°** **(−30° to 31°)**	(−57° to 24°) Ant. 1 (−23° to 60°) Ant. 2 **Total = 117°** **(−57° to 60°)**
xz-plane	y-directed E-field (*V-pol*)	(−32° to 0°) Ant. 4 (0° to 29°) Ant. 3 **Total = 61°** **(−32° to 29°)**	(−58° to 23°) Ant. 4 (−22° to 59°) Ant. 3 **Total = 117°** **(−58° to 59°)**

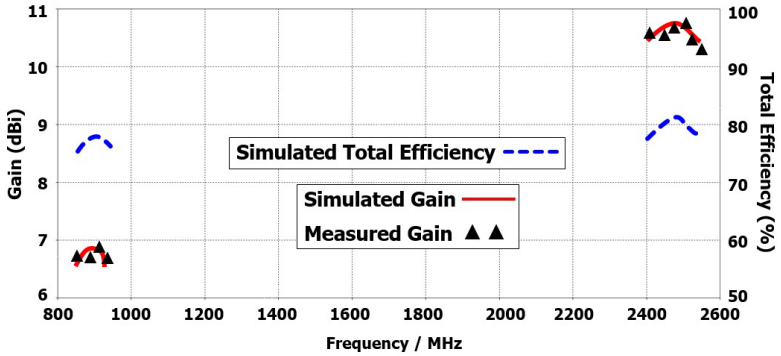

FIGURE 11. Gain and total efficiency vs. frequency for Ant. 1.

plane (*V-pol*). The 3 dB beamwidth has twice the scan range, with 117° both in the *yz*- and *xz*-planes.

5. COMPARISON WITH EXISTING DESIGNS

Table 3 provides a comparison between recent dual-band RFID readers and the proposed work.

It is noted that the proposed antenna uses only a single substrate layer, giving it the lowest profile. This makes the antenna lightweight. The proposed antenna covers both the North-American and European UHF-RFID bands. Thus, it can be utilized to detect a wide variety of tags. Thirdly, the antenna has high gain in all the operational bands. The antenna designed in [21] has similar gains while the RFID reader presented in [3] has better gains. However, both these readers trade off their profile heights to achieve the gains. Finally, the main highlight of this antenna system is the frequency-dependent beam scanning nature within the WLAN/Microwave-RFID band. This sets the antenna apart from existing dual-band RFID readers available in literature.

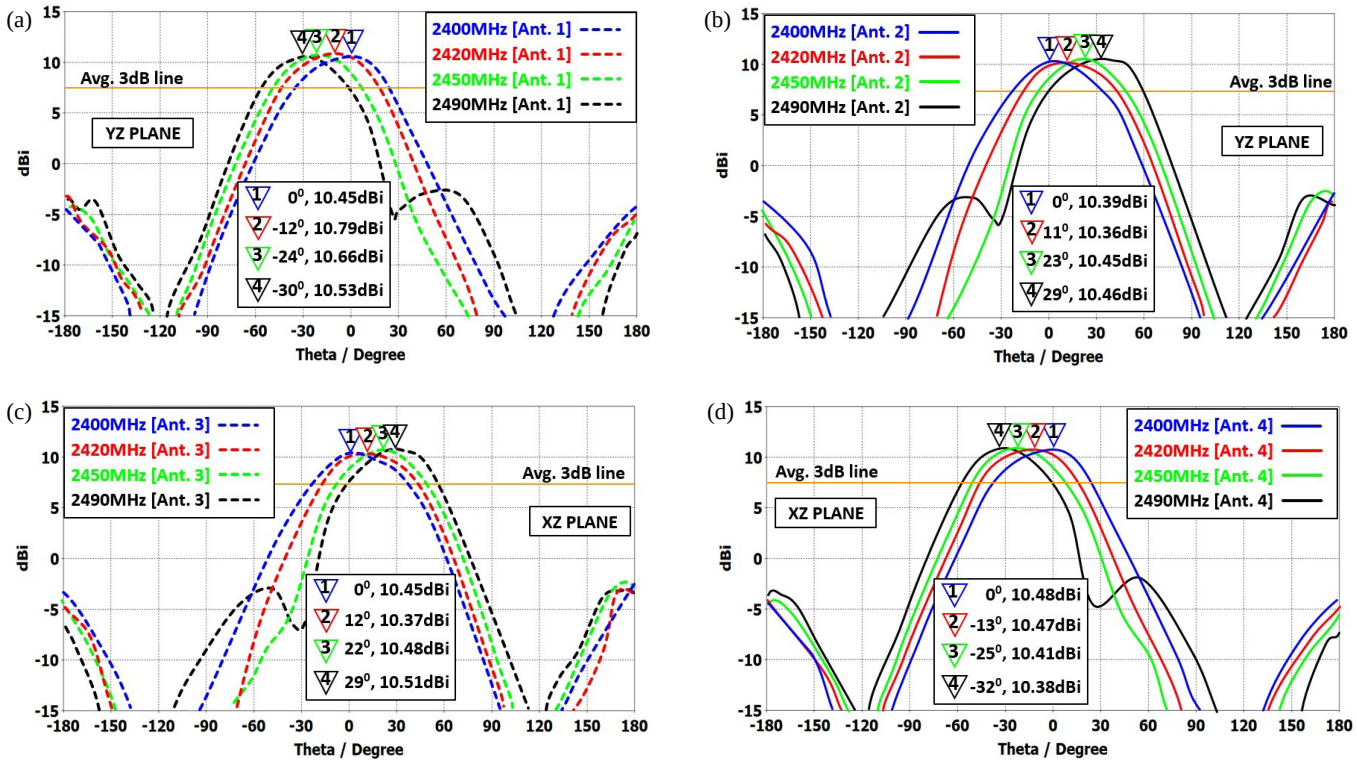

FIGURE 12. Measured horizontally polarized beam scanning along the *yz*-plane by (a) Ant. 1 and (b) Ant. 2. Measured vertically polarized beam scanning along the *xz*-plane by (c) Ant. 3 and (d) Ant. 4.

TABLE 3. Comparisons with existing dual-band RFID readers.

Ref.	Bands (GHz)	Size at lowest freq.	Gain dBi	No. of substrates	Beam scanning
[17]	0.915 2.45	$0.64 \times 0.64 \times 0.09\lambda_0^3$	3.1 6.25	2	No
[21]	0.92 2.45	$0.42 \times 0.42 \times 0.09\lambda_0^3$	6.02 9.14	3	No
[10]	0.92 2.45	$0.24 \times 0.24 \times 0.024\lambda_0^3$	3.3 5	3	No
[3]	0.92 2.45	$0.82 \times 0.82 \times 0.11\lambda_0^3$	8.8 13.3	4	No
This work	**0.865** **0.914** **2.45**	$\mathbf{0.71 \times 0.71 \times 0.004\lambda_0^3}$	**6.68** **6.78** **10.4**	**1**	**Yes** **2.45 GHz**

6. CONCLUSION

A 2×2 multiport single-layered microstrip patch antenna system is presented in this paper. The antenna system can simultaneously cover both the European and North-American UHF-RFID bands (860–930 MHz) with good gain (around 7 dBi) and efficiency (75–80%). The reader is dual-linearly polarized within this band. Moreover, the antenna system can perform frequency-dependent beam scanning in both the *xz*- and *yz*-planes within the WLAN/Microwave-RFID band (2400–2500 MHz).

REFERENCES

[1] Finkenzeller, K., *RFID Handbook: Fundamentals and Applications in Contactless Smart Cards, Radio Frequency Identification and Near-field Communication*, 3rd ed., John Wiley & Sons, Hoboken, NJ, USA, 2010.

[2] Sarkar, S., "Three dual-band and dual-linearly polarized antenna configurations for UHF-RFID and WLAN applications," *IEEE Journal of Radio Frequency Identification*, Vol. 8, 571–579, 2024.

[3] Xu, R. and Z. Shen, "Dual-band circularly polarized RFID reader antenna with combined dipole and monopoles," *IEEE Transactions on Antennas and Propagation*, Vol. 71, No. 12, 9593–9600, Dec. 2023.

[4] Liu, Q., J. Shen, J. Yin, H. Liu, and Y. Liu, "Compact 0.92/2.45-GH dual-band directional circularly polarized microstrip antenna for handheld RFID reader applications," *IEEE Transactions on Antennas and Propagation*, Vol. 63, No. 9, 3849–3856, Sep. 2015.

[5] Liu, X., S. Fang, and H. Liu, "A compact dual-band circularly polarized RFID reader/WLAN antenna," in *Proceedings of the 2021 9th International Conference on Communications and Broadband Networking*, 269–273, Shanghai, China, 2021.

[6] Li, J., H. Liu, S. Zhang, M. Luo, Y. Zhang, and S. He, "A wideband single-fed, circularly-polarized patch antenna with enhanced axial ratio bandwidth for UHF RFID reader applications," *IEEE Access*, Vol. 6, 55 883–55 892, 2018.

[7] Caso, R., A. Michel, M. Rodriguez-Pino, and P. Nepa, "Dual-band UHF-RFID/WLAN circularly polarized antenna for portable RFID readers," *IEEE Transactions on Antennas and Propagation*, Vol. 62, No. 5, 2822–2826, May 2014.

[8] Kumar, D. and N. Jaglan, "A dual band circularly polarized RFID reader antenna for Internet of Things application," in *2023 9th International Conference on Signal Processing and Communication (ICSC)*, 13–16, Noida, India, Dec. 2023.

[9] Panda, J. R. and R. S. Kshetrimayum, "A printed 2.4 GHz/5.8 GHz dual-band monopole antenna with a protruding stub in the ground plane for WLAN and RFID applications," *Progress In Electromagnetics Research*, Vol. 117, 425–434, 2011.

[10] Bajaj, C., D. K. Upadhyay, S. Kumar, and B. K. Kanaujia, "A dual-band circularly polarized hexagonal ring antenna for handheld RFID readers," *Wireless Personal Communications*, Vol. 125, No. 4, 3101–3115, 2022.

[11] Wang, Z., R. She, J. Han, S. Fang, and Y. Liu, "Dual-band dual-sense circularly polarized stacked patch antenna with a small frequency ratio for UHF RFID reader applications," *IEEE Access*, Vol. 5, 15 260–15 270, 2017.

[12] Zhang, W.-H., P. Cheong, W.-J. Lu, and K.-W. Tam, "Planar end-fire circularly polarized antenna for low profile handheld RFID reader," *IEEE Journal of Radio Frequency Identification*, Vol. 2, No. 1, 15–22, Mar. 2018.

[13] Choi, J., U. Kim, Y. Um, and D. Shin, "Design of antennas for the UHF RFID system," in *2008 International Workshop on Antenna Technology: Small Antennas and Novel Metamaterials*, 75–78, Chiba, Japan, Mar. 2008.

[14] Xu, R., J. Liu, K. Wei, W. Hu, Z.-J. Xing, J.-Y. Li, and S. S. Gao, "Dual-band circularly polarized antenna with two pairs of crossed-dipoles for RFID reader," *IEEE Transactions on Antennas and Propagation*, Vol. 69, No. 12, 8194–8203, 2021.

[15] Lai, F.-P., J.-F. Yang, and Y.-S. Chen, "Compact dual-band circularly polarized antenna using double cross dipoles for RFID handheld readers," *IEEE Antennas and Wireless Propagation Letters*, Vol. 19, No. 8, 1429–1433, Aug. 2020.

[16] Ojaroudi Parchin, N., H. J. Basherlou, R. A. Abd-Alhameed, and J. M. Noras, "Dual-band monopole antenna for RFID applications," *Future Internet*, Vol. 11, No. 2, 31, 2019.

[17] Sarkar, S. and B. Gupta, "A dual-band circularly polarized antenna with a dual-band AMC reflector for RFID readers," *IEEE Antennas and Wireless Propagation Letters*, Vol. 19, No. 5, 796–800, May 2020.

[18] Panda, J. R., A. S. R. Saladi, and R. S. Kshetrimayum, "A compact printed monopole antenna for dual-band RFID and WLAN applications," *Radioengineering*, Vol. 20, No. 2, 464–467, Jun. 2011.

[19] Huang, T.-J. and H.-T. Hsu, "A high-gain circularly-polarized dual-band antenna array for RFID reader applications," in *2012 IEEE International Workshop on Electromagnetics: Applications and Student Innovation Competition*, 1–2, Chengdu, China, Aug. 2012.

[20] Sarkar, S. and B. Gupta, "A dual frequency circularly polarized UHF-RFID/WLAN circular patch antenna for RFID readers," in *2019 IEEE International Conference on RFID Technology and Applications (RFID-TA)*, 448–452, Pisa, Italy, Sep. 2019.

[21] Wang, X., Z. Xing, Z. Zhao, J. Li, and Q. Yu, "Dual-band polarization conversion metasurface-assisted compact high-efficiency RFID reader antenna design," *IEEE Transactions on Antennas and Propagation*, Vol. 72, No. 11, 8810–8815, Nov. 2024.